ОПТИЧЕСКИЙ ЖУРНАЛ. 2023. Том 90. № 9. С. 82–90
OPTICHESKII ZHURNAL. 2023. V. 90. № 9. Pp. 82–90

Научная статья
Research Article

Оптический журнал
Оптическое приборостроение и метрология
Optical instrument making and metrology

DOI: 10.17586/1023-5086-2023-90-09-82-90
УДК 535.8

Design and simulation of a fiber sensing system for metal ion detection based on side-polished fiber and coated fiber grating

JunQi Guo[1], YanFang Zhou[2], Yu Liu[3], ChangLe Wang[4], WenYue Zheng[5], JinLu Jiang[6], HanYing Ji[7], XiaoYu Chen[8], RenPu Li[9]✉

Chongqing University of Post and Telecommunications, Chongqing, China

[1]*guojq@cqupt.edu.cn* *https://orcid.org/0000-0001-9570-530X*
[2]*1985430650@qq.com* *https://orcid.org/0009-0002-3634-1280*
[3]*liuyu@cqupt.edu.cn* *https://orcid.org/0000-0001-6929-1481*
[4]*1016007806@qq.com* *https://orcid.org/0009-0000-0137-7473*
[5]*308649700@qq.com* *https://orcid.org/0009-0007-2616-2461*
[6]*1845426516@qq.com* *https://orcid.org/0009-0005-8559-0533*
[7]*1529978166@qq.com* *https://orcid.org/0009-0004-4511-3444*
[8]*1241655631@qq.com* *https://orcid.org/0009-0004-2846-2028*
[9]*lirp@cqupt.edu.cn* *https://orcid.org/0000-0002-0426-296X*

Abstract

Subject of study. A fluid metal ion detection device is designed to solve the issue of heavy metal water quality detection in real life, which is used by a fusion of a side-throw fiber-assisted fluid structure and a long-period fiber grating coated with a metal chelator film. The **aim of the work** is to design of a fiber-optic fluid system for the simultaneous qualitative and quantitative analysis of metal ions in a liquid. **Method.** The refractive index bands of common contaminated water sources are selected for the numerical simulation of metal ion species and concentration sensing characteristics. **Main results.** The results show that the interference wavelength is red-shifted with the increase of the filled fluid concentration. Its refractive index sensing sensitivity is calculated to be about 3343.33 nm/RIU. Meanwhile, when the refractive index of long-period fiber grating film layer increases from 1.2 to 1.44, the loss peak decreases by a total of 6.011 dB, and thus the ion species can be identified. **Practical significance.** Therefore, this sensing system offers the possibility of real-time detection of fluid ion orientation.

Keywords: optofluidic system, optical fiber sensing, microstructured optical fiber, metal ion detection

Acknowledgment: the work was funded by the National Natural Science Foundation of China (61705027, 62005033, and 52175531), Chongqing Science and Technology Commission Basic Research Project (CSTC-2020jcyj-msxm0603), Chongqing Municipal Education Commission Science and Technology Research Program (KJQN202000609).

For citation: Guo J.Q., Zhou Ya.F., Liu Yu, Wang C.L., Zhen W.Yu., Jiang J.L., Ji H.Y., Chen X.Yu, Li R.P. Design and simulation of a fiber sensing system for metal ion detection based on side-polished fiber and coated fiber grating [in English] // Opticheskii Zhurnal. 2023. V. 90. № 9. P. 82–90. http://doi.org/10.17586/1023-5086-2023-90-09-82-90

OCIS code: 060.2370

Моделирование и проектирование волоконной сенсорной системы для обнаружения ионов металлов на основе оптического волокна с боковой полировкой и волоконной решетки с покрытием

JunQi Guo[1], YanFang Zhou[2], Yu Liu[3], ChangLe Wang[4], WenYue Zheng[5], JinLu Jiang[6], HanYing Ji[7], XiaoYu Chen[8], RenPu Li[9]✉

Chongqing University of Post and Telecommunications, Chongqing, China

[1]guojq@cqupt.edu.cn https://orcid.org/0000-0001-9570-530X
[2]1985430650@qq.com https://orcid.org/0009-0002-3634-1280
[3]liuyu@cqupt.edu.cn https://orcid.org/0000-0001-6929-1481
[4]1016007806@qq.com https://orcid.org/0009-0000-0137-7473
[5]308649700@qq.com https://orcid.org/0009-0007-2616-2461
[6]1845426516@qq.com https://orcid.org/0009-0005-8559-0533
[7]1529978166@qq.com https://orcid.org/0009-0004-4511-3444
[8]1241655631@qq.com https://orcid.org/0009-0004-2846-2028
[9]lirp@cqupt.edu.cn https://orcid.org/0000-0002-0426-296X

Аннотация

Предмет исследования. Устройство для обнаружения и измерения концентрации ионов тяжелых металлов в жидкости при контроле качества воды, состоящее из структуры, взаимодействующей с жидкостью в виде волокна с боковой полировкой, и длиннопериодной волоконной решетки, покрытой хелатированной металлической пленкой. **Цель работы.** Разработка волоконно-оптической жидкостной системы для одновременного качественного и количественного анализа ионов металлов в растворе. **Метод.** Компьютерное моделирование зависимости показателя преломления воды при наличии загрязнения от концентрации ионов и вида металла с последующим макетированием сенсора. **Основные результаты.** Установлено смещение длины волны интерференции, возникающей в волоконных элементах сенсора в длинноволновую область спектра при увеличении концентрации примесей в воде. При этом расчетная чувствительность сенсора к изменению показателя преломления контролируемой среды составляет 3343,33 нм/RIU[1], что позволяет измерять концентрацию примеси. Доказана возможность идентификации вида ионов примеси по уменьшению потерь излучения, достигающему в общей сложности 6,011 дБ при изменении показателя преломления пленочного покрытия длиннопериодной волоконной решетки сенсора в интервале от 1,2 до 1,44. **Практическая значимость.** Доказана возможность реализации высокоточного волоконного сенсора для оперативного контроля загрязнения воды ионами тяжелых металлов в реальном времени.

Ключевые слова: оптико-жидкостная система, оптоволоконный сенсор, микроструктурированное оптическое волокно, обнаружение ионов металла

Благодарность: в финансировании проведения работы участвовали Национальный фонд естественных наук Китая (61705027, 62005033 и 52175531), Проект фундаментальных исследований Чунцинской комиссии по науке и технологиям (CSTC-2020jcyj-msxm0603), Программа научно-технических исследований Муниципальной комиссии по образованию Чунцина (KJQN202000609).

Ссылка для цитирования: Guo J.Q., Zhou Ya.F., Liu Yu, Wang C.L., Zhen W.Yu., Jiang J.L., Ji H.Y., Chen X.Yu, Li R.P. Design and simulation of a fiber sensing system for metal ion detection based on side-polished fiber and coated fiber grating (Моделирование и проектирование волоконной сенсорной системы для обнаружения ионов металлов на основе оптического волокна с боковой полировкой и волоконной решетки с покрытием) [на англ. яз.] // Оптический журнал. 2023. Т. 90. № 9. С. 82–90. http://doi.org/10.17586/1023-5086-2023-90-09-82-90

Код OCIS: 060.2370

[1] RIU — минимально обнаруживаемое изменение показателя преломления поверхности, по которой распространяется затухающая волна.

INTRODUCTION

As issues with water pollution worsen, it is crucial to develop techniques for detecting the heavy metal content of the water. Atomic spectral absorption [1], anodic dissolution voltammetry [2], chemical sensing [3], optical fiber sensing [4, 5], etc. are currently the most popular detection techniques for metal contaminants in solution. The optical fiber sensor has its own intrinsic features of simple structure, stability, corrosion resistance, and high sensitivity, when utilized for water pollution detection [6–9]. Therefore, studying a new kind of sensor for real-time and directional fluid ion detection is extremely important for both academic research and practical applications.

Many ion detection techniques based on fiber optic sensors have been reported in recent years. In 2020, Cai S. et al. made a highly sensitive plasma light probe based on a gold-plated tilted fiber Bragg grating capable of selectively detecting Cd^{2+} concentrations down to 1 ppb [10]. In 2021, Kavitha et al. used a functionalized fiber Bragg grating to make an ion probe that can specifically identify Hg^{2+} ions among many ions containing Pb^{2+}, Cu^{2+}, Na^{2+}, Cd^{2+}, etc. with a detection limit of 100 nm [11]. In 2022, Li G. et al. spliced a hydrogel-coated few-mode fiber between two coreless fibers and used the hydrogel's specificity in conjunction with the modal interference fiber sensing principle to detect the presence of Pb^{2+} in water with a sensing sensitivity of 8.155×10^5 nm/(mol/L) [12]. In conclusion, the optical fiber solution detection technique is effective in designing fluid sensors with high sensitivity and novel sensing principles. However, the above structures can typically only detect one type of ion, and the ion fiber optic sensors cannot concurrently identify the species and concentration of ions in low refractive index contaminated fluid.

This paper provides a photonic crystal fiber optic fluid sensing structure based on a coated long-period fiber grating (LPFG) and a side-polished fiber-assisted opening. Since changes of the filling refractive index leads to changes of the birefringence, the birefringence theory is utilized to detect metal ion concentrations in photonic crystal fiber. Changes in the external environment or the film layer of the coated fiber grating will change the grating mode coupling, so the chelation reaction can be utilized to identify specific metal ion species. Additionally, the length and depth of the side-polished fiber can be controlled, and its large open liquid channel can realize the operation of changing and mixing the liquid to be measured. This system provides the possibility of real-time monitoring of heavy metal ion contamination. This structure can be used for heavy ion water contamination detection, which allows the concentration and type of ions to be detected, while maintaining the fluidity of the solution.

The aim of the work is to design of a fiber-optic fluid system for the simultaneous qualitative and quantitative analysis of metal ions in a liquid.

SYSTEM ARCHITECTURE DESIGN

In order to achieve the detection of heavy metal ion contamination in fluids, the system structure provided in this paper is depicted in Fig. 1. It's made up of a fiber grating structure, a photonic crystal fiber optic fluid structure, a light source, a spectrometer, a 3dB coupler, and a polarizer. Real-time monitoring of the metal ion concentration in the fluid can be measured using a photonic crystal fiber optic fluid system with birefringence effect and huge open channel. The concentration sensing sensitivity can be ensured by combining this structure with

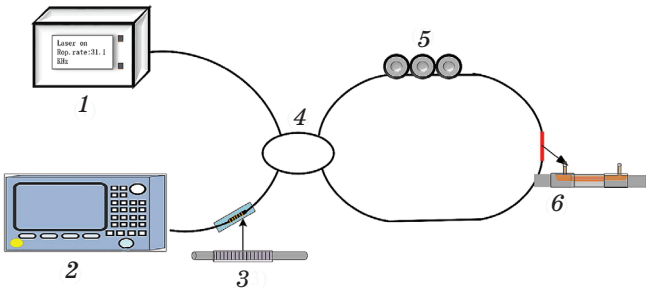

Fig. 1. Schematic diagram of the new optofluidic control system. (*1*) Light source (laser), (*2*) spectrometer, (*3*) long period fiber grating coated with chelated metal film, (*4*) 3dB coupler, (*5*) polarization controller, (*6*) fluid systems

Рис. 1. Принципиальная схема новой оптико-жидкостной системы контроля. Источник света (лазер) — *1*, спектрометр — *2*, длиннопериодная волоконная решетка, покрытая хелатированной металлической пленкой — *3*, ответвитель 3 дБ — *4*, контроллер поляризации — *5*, жидкостные системы — *6*

the Sagnac interferometer. The chelation reaction of the coated fiber grating can assist us in identifying the metal ion species present in the fluid. As a result, this technology presents a viable approach to achieving the directional detection of fluid ions.

In the fluid systems, side-polished fibers (SPF) are used to assist photonic crystal fiber (PCF) to form fluid sensors with SPF–PCF–SPF structure. This operation not only increases the fluid inlet, but also enables the replacement and mixing of the material to be measured. Sagnac interferometer is used in conjunction with SPF–PCF–SPF structure since the refractive index of contaminated water in real life is typically lower than the refractive index of the substrate material of optical fiber, and Sagnac interferometer has high sensitivity for low refractive index sensing. The SM-28 fiber from Wuhan Changfei Company is used as the reference model for the side-polished fiber with the cladding and core diameters of 125 and 9 μm respectively. Light-guiding characteristics of polished fibers are simulated using COMSOL software. Figure 2 displays the simulation results. From the graph we can see the optical signal is well contained within the core at this polishing depth. The photonic crystal fiber model refers to PCF-125-03 from Wuhan Changfei with a cladding diameter of 135 μm. Cladding air pores with a diameter of 35 μm are regularly arranged in a square hexagonal shape. The air hole pitch is 4.9 nm. The SPF–PCF–SPF simulation model is shown in Fig. 3, the polishing depth of the side-polished fiber is 57 μm to ensure that the PCF just exposes the 5 layers of air holes.

Figure 4 depicts the completed SPF–PCF–SPF fiber optic fluid sensing system. The two sections

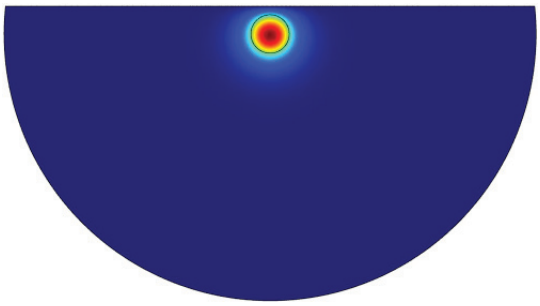

Fig. 2. Simulation result of side-polished fiber

Рис. 2. Результаты моделирования конструкции оптического волокна с боковой полировкой

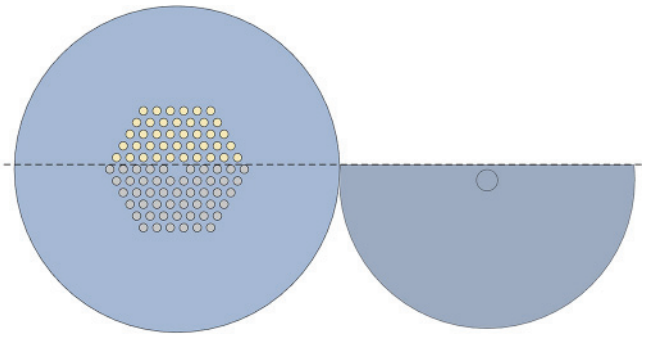

Fig. 3. Simulation model of SPF–PCF–SPF

Рис. 3. Результаты моделирования конструкции структуры «оптическое волокно с боковой полировкой – оптическое волокно с центральной полировкой – оптическое волокно с боковой полировкой»

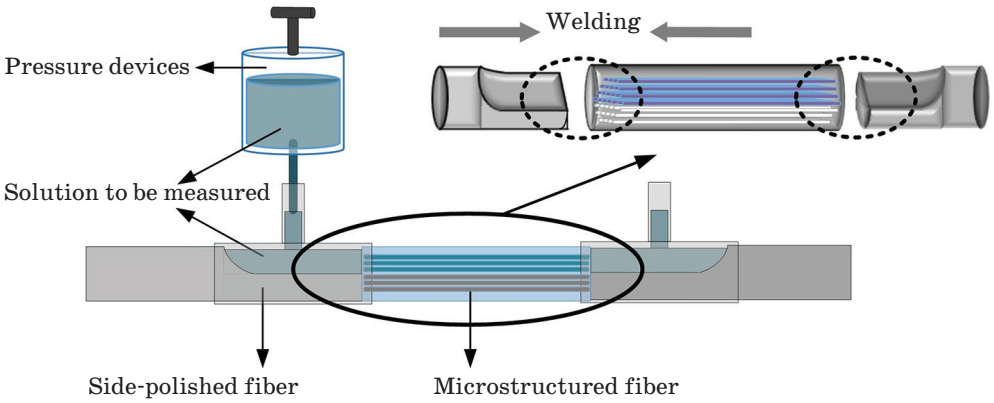

Fig. 4. Scheme of the structure of SPF–PCF–SPF

Рис. 4. Схема общей структуры «оптическое волокно с боковой полировкой — оптическое волокно с центральной полировкой — оптическое волокно с боковой полировкой»

of the polished optical fiber are fused to the two ends of the photonic crystal fiber to ensure the same number of layers of air holes exposed at the fused end face. A pressure booster is attached to the vertical end of the tee tube, which is inserted in the fiber polishing area, and it is used to fill and replace the measurement liquid. This structure realizes the channel with large opening and solves the problem that some optofluidic systems are difficult to fill due to the small opening. Meanwhile, the double-sided opening structure allows for fluid material replacement and real-time monitoring of fluid sensing.

The above SPF–PCF–SPF structure allows the filling of part of the air holes of the photonic crystal fiber, introducing a large asymmetry, so that the refractive index of the filled fluid can be detected based on the principle of birefringence. The relationship between ion concentration c and refractive index n can be described according to Lorenz's law and the Beer–Lambert theoretical model as follows: The relationship between c and n can be roughly calculated as when the incident light frequency is fixed. That is, the fluid sensing structure can monitor fluid material concentration in real time.

The above content only realizes the detection of fluid ion concentration, and then the specific recognition functions of fluid ion species is studied. Figure 5 depicts the structure of the coated LPFG. Directional recognition of ionic species is accomplished by the chelation reaction of coated LPFG with metal ions.

The film material can have specific chelating reactions with the metal ions to be detected.

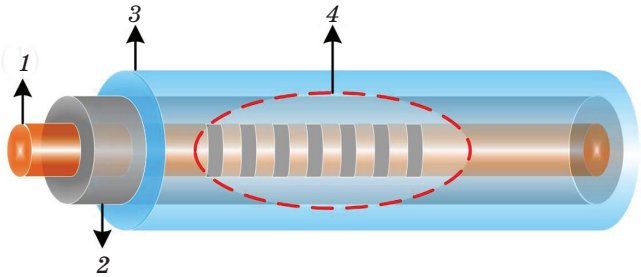

Fig. 5. The structure of coated LPFG. (*1*) Core, (*2*) cladding, (*3*) coating layer, (*4*) LPFG

Рис. 5. Структура длиннопериодной волоконной решетки, покрытой хелатированной металлической пленкой. *1* — сердцевина, *2* — оболочка, *3* — слой покрытия, *4* — длиннопериодная волоконная решетка

The reaction between the film and the ion to be measured results in the formation of a corresponding chelate attached to the film layer, causing changes in the refractive index of the film. Changes in the refractive index of the film and the environment cause regular changes in the resonant wavelength and loss peak amplitude. In other words, recognition of metal ion species can be achieved with the aid of coated LPFG.

In conclusion, this paper proposes a system for fusing a coated fiber grating sensing structure with a photonic crystal fiber optic fluidic structure. This structure can detect ion concentration using the birefringence phenomenon generated by the SPF–PCF–SPF structure, while the coated fiber grating structure can identify ions. Therefore, the system has a directional detection function for fluid ion characteristics.

THEORETICAL MODELLING AND NUMERICAL SIMULATION ANALYSIS

The viability of the system structure is examined in this research using theoretical and numerical simulations. To achieve real-time detection of fluid ion concentration, a theoretical model of photonic crystal fiber fluid structure based on Sagnac interferometry and photonic crystal fiber birefringence phenomenon is presented. Meanwhile, a thorough investigation is made into the birefringence phenomenon caused by the asymmetric fluid filling of the photonic crystal fiber.

The Sagnac interferometer is often used in all-optical devices due to its simple structure and high sensitivity [13–15]. In the numerical simulations of this structure, the ensuing equations are applied: the transmission spectrum expression of Sagnac is shown in Eqs. (1) and (2), and the birefringence is shown in Eq. (3)

$$T = \left[1 - \cos(\varphi)\right]/2, \tag{1}$$

$$\varphi = 2\pi l B(\lambda)/\lambda, \tag{2}$$

$$B(\lambda) = \mathrm{Re}\left|n_{\mathrm{eff}}^{y}(\lambda) - n_{\mathrm{eff}}^{x}(\lambda)\right|. \tag{3}$$

Here, φ is the phase differences, l is the fluid fill length, λ is the wavelength in vacuum, Re represents the real part, $n_{\mathrm{eff}}^{x}(\lambda)$ and $n_{\mathrm{eff}}^{y}(\lambda)$ are the effective refractive indexes of the core

in the x-polarization and y-polarization respectively. From the above equations it can be concluded that as the refractive index of the filled solution changes, the birefringence changes, and ultimately leads to a change in the Sagnac interference spectrum.

This paper combines the water solubility of heavy metal ions, as well as the fact that the refractive index of the polluted water source in life is generally lower than the refractive index of the optical fiber substrate material. The fluid material with a refractive index range of 1.333 to 1.351 is chosen to be filled into the SPF–PCF–SPF structure. The simulation is performed with COMSOL, and the structure parameters are established in accordance with the PM-PCF-125-10 fiber from Wuhan Changfei Company. Figure 6 illustrates the mode birefringence at 1300 nm in the common communication band, and the calculation results show that when the refractive index of the filled liquid increases, the birefringence becomes higher. Thus, this system can produce an effective birefringence effect by filling the liquid asymmetrically.

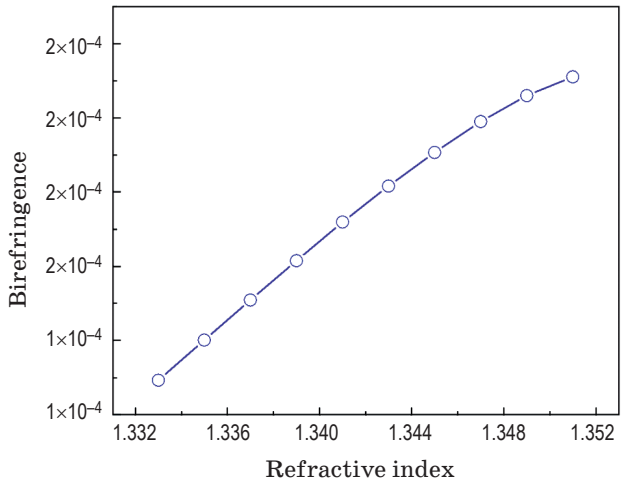

Fig. 6. Variation curve of birefringence with refractive index of filled liquid. Wavelength 1300 nm

Рис. 6. График функции изменения двулучепреломления в зависимости от показателя преломления жидкости, которой заполнена система. Длина волны 1300 нм

The transmission spectrum of Sagnac interferometer filled with different fluid refractive indices is obtained, as shown in Fig. 7a.

As seen in the Fig. 7a, the wavelength of the resonant peak is red-shifted as the refractive index of the filled liquid increases. The highest point on the resonant peak waveform is chosen as the data observation point, and the wavelength variation curve with refractive index at that point is obtained, as shown in Fig. 7b. The wavelength of the observation point shifts by a total of 60.18 from 1300.41 to 1362.59 nm, when the refractive index rises from 1.333 to 1.351. The calculated refractive

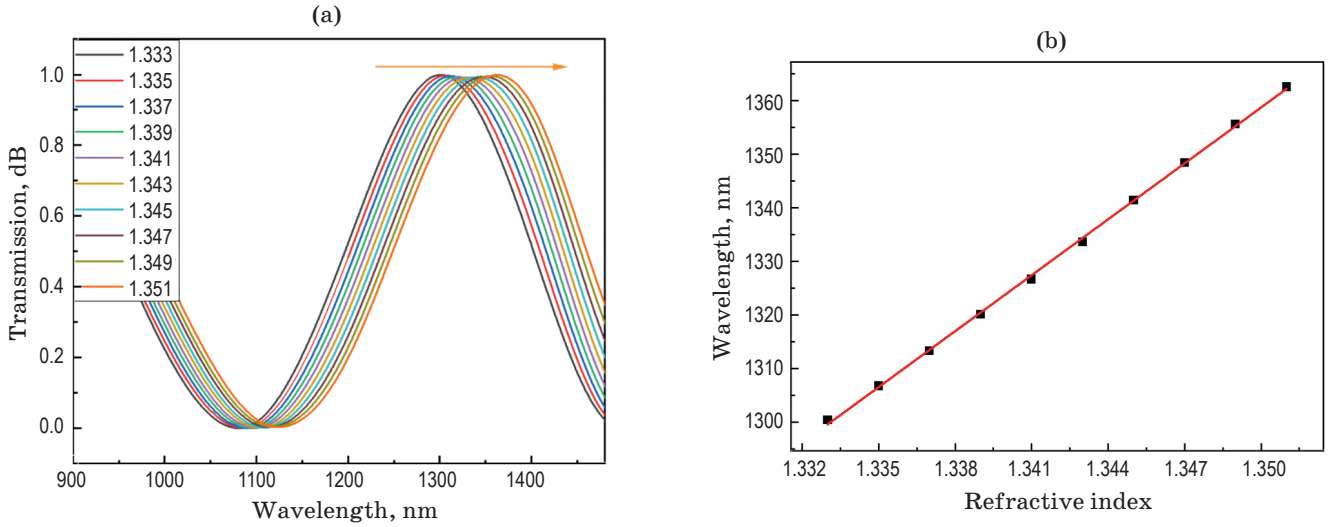

Fig. 7. (a) Transmission spectra of liquid-filled fiber Sagnac interferometer (in the inset of Fig. 7a, the refractive indices corresponding to the curves) and (b) refractive index fitting curves

Рис. 7. Спектры пропускания волоконного интерферометра Саньяка (a), заполненного жидкостью, и графики отклонения показателя преломления жидкости (b). На вставке рис. 7a соответствующие кривым показатели преломления

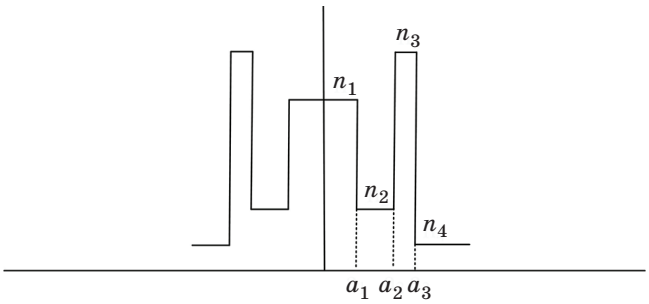

Fig. 8. Refractive index distribution. Explanations are in the text

Рис. 8. Распределение коэффициента преломления. Пояснения в тексте

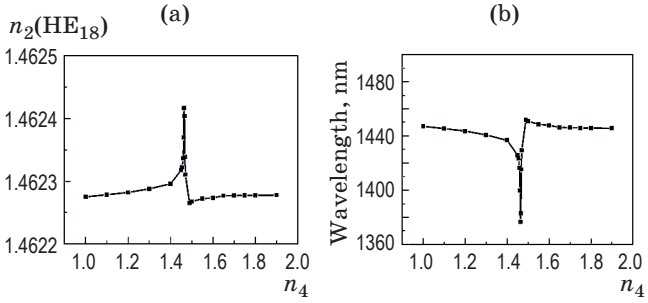

Fig. 9. (a) HE_{18} cladding pattern effective refractive index variation curve, (b) resonant wavelength variation curve

Рис. 9. График изменения эффективного показателя преломления оболочки HE_{18} (a), резонанс при изменении длины волны (b)

index sensing sensitivity of the system is about 3343.33 nm/RIU[2]. Resonant wavelength fluctuation vs refractive index variation is linearly fitted with a 99.94% fit. It is demonstrated that the method can be utilized to identify fluids with low refractive index.

In order to realize the function of directional identification of fluid ion species, theoretical aspects of coated LPFG sensing are investigated. The impact of external and film layer refractive index changes on the coupling of coated LPFG modes are examined. The refractive index distribution of the coated LPFG is shown in Fig. 8, where n_1, n_2, n_3, and n_4 are the refractive indices of the core, cladding, coating layer, and external environment respectively. a_1 is the radius of the core layer, a_2 is the radius of the cladding layer, and a_3 is the radius of the coating layer, so the coating thickness satisfies $h = a_3 - a_2$ and the refractive index satisfies $n_3 > n_1 > n_2$.

According to the coupling theory of fiber grating, it can be concluded that LPFG satisfies the following phase conditions

$$\lambda_{res} = (n_{eff}^{co} - n_{eff}^{cl})\Lambda, \quad (4)$$

where λ_{res} is the resonant wavelength, n_{eff}^{co} is the effective refractive index of the core, n_{eff}^{cl} is the effective refractive index of the cladding mode, and Λ is the period of the fiber grating. When the external environment, such as temperature, strain, environmental refractive index changes, the grating period, length and refractive index of the fiber core and cladding layer will change. These changes will also change the LPFG mode coupling, which will lead to changes in the grating transmission spectrum, and ultimately manifest as changes in resonant wavelength and loss peak amplitude.

MATLAB is utilized for the numerical analysis in this paper, and only the value of n_4 is altered to find the values of n_{eff}^{co} and n_{eff}^{cl} for each order of 1 under various ambient refractive indices. Take HE_{18} cladding mode as an example for analysis, the result is shown in Fig. 9a. The influence curve of the ambient refractive index on the resonant wavelength is then obtained by substituting the data into Eq. (4), as illustrated in Fig. 9b.

According to Fig. 9a, n_{eff}^{cl} rises as n_4 rises. When n_4 is very close to the n_{eff}^{cl}, n_{eff}^{cl} changes dramatically, rising quickly, falling quickly, and then slowly increasing again. As shown in Fig. 9b, as n_4 increases, λ_{res} first drifts in the short-wave direction, and the closer n_4 is to n_{eff}^{cl}, the larger this drift is, and near $n_4 = n_{eff}^{cl}$, λ_{res} jumps, and then followed by a slow drift towards the shortwave direction with increasing n_4, but is always greater than the resonant wavelength at $n_4 = 1$.

The change in the resonant peak waveform of the coated LPFG is also simulated by changing only the value of n_3 for the case $n_4 = 1$. The outcomes are displayed in Fig. 10.

As can be seen from Fig. 10, when the refractive index of the film layer increases, the wavelength of the resonant peak is slightly blue-shifted, while the amplitude of the loss peak decreases significantly. The depth of the loss peak reduced from –21.062 to –15.051 dB as the

[2] Refractive index unit.

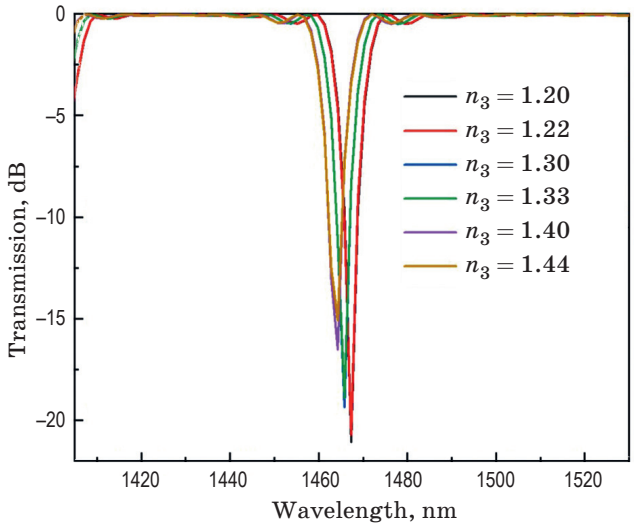

Fig. 10. Plated LPFG resonance peak variation curve

Рис. 10. Резонанс при изменении длины волны длиннопериодной волоконной решетки, покрытой хелатированной металлической пленкой

refractive index of the film layer rose from 1.2 to 1.44, with a total reduction of 6.011 dB. It can be seen that the change in refractive index of the film layer has a certain influence on the loss peak amplitude, which proves that the structure can distinguish between different metal ion species.

In conclusion, numerical simulations of the SPF–PCF–SPF structure and the coated LPFG structure are performed in this paper. The results demonstrate that the chelation reaction can be used to directionally identify metal ion species, while the birefringence theory can be used to detect metal ion concentration. Currently, the structure proposed in this paper does not allow for species identification of various metal ions, but this issue can be solved by changing the different chelating agents. The specific implementation scheme needs to be further studied. As a result, this system offers a workable solution for carrying out the detection of different metal ions in fluids.

CONCLUSION

In this paper, the new fused optical fiber fluid sensing system based on coated LPFG and side-polishing optical fiber is theoretically proposed. The birefringence phenomenon generated by the SPF–PCF–SPF structure can achieve the detection of ion concentration, and the function of the ion species recognition can be implemented by the coated LPFG structure. Simulation results show that the Sagnac interferometer refractive index sensing sensitivity of the fluid system is about 3343.33 nm/RIU, and the loss peak is reduced by a total of 6.011 dB, when the refractive index of the film layer is increased from 1.2 to 1.44. The system is not only simple in structure, but also successfully achieves directional detection of fluid ions. It can be applied not only for heavy metal ion detection in water pollution, but it can also be researched further in the areas of biomedicine and chemical reaction processes for additional sensing systems.

REFERENCES

1. Zhou K., Liu Z., Cong M., et al. Detection of chemical oxygen demand in water based on UV absorption spectroscopy and pso-lssvm algorithm // J. Optoelectron. Lett. 2022. V. 18. № 4. P. 0251–2056. https://doi.org/10.1007/s11801-022-1143-5
2. Lu Y., Liang X., Niyungeko C., et al. A review of the identification and detection of heavy metal ions in the environment by voltammetry // Talanta. 2018. V. 178. P. 324–338. https://doi.org/10.1016/j.talanta.2017.08.033
3. Sun C., Ou X., Cheng Y., et al. Coordination-induced structural changes of DNA-based optical and electrochemical sensors for metal ions detection // Dalton Trans. 2019. V. 48. № 18. P. 5879–5891. https://doi.org/10.1039/C8DT04733B
4. Si Y., Lao J., Zhang X., et al. Electrochemical plasmonic fiber-optic sensors for ultra-sensitive heavy metal detection // J. Lightw. Technol. 2019. V. 37. № 14. P. 3495–3502. http://doi.org/10.1109/JLT.2019.2917329
5. Shakya A.K., Singh S. State of the art in fiber optics sensors for heavy metals detection // J. Opt. and Laser Technol. 2022. V. 153. P. 1879–2545. https://doi.org/10.1016/j.optlastec.2022.108246
6. Pan J.H., Cao C., Zhang A., et al. A high sensitivity localized surface plasmon resonance sensor based on D-shaped photonic crystal fiber for low refractive index detection // J. Optoelectron. Lett. 2022. V. 18. № 7. P. 425–429. https://doi.org/10.1007/s11801-022-1193-8
7. Zain H.A., Batumalay M., Rahim H.R.A., et al. Single-walled carbon nanotubes coated D-shaped fiber for aqueous ethanol detection // J. Optoelectron. Lett. 2022. V. 18. № 7. P. 430–433. https://doi.org/10.1007/s11801-022-1166-y
8. Bashan G., London Y., Diamandi H.H., et al. Distributed cladding mode fiber-optic sensor // Optica. 2020. V. 7. № 1. P. 85–92. https://doi.org/10.1364/OPTICA.377610
9. Blakley S., Liu X., Fedotov I., et al. Fiber-optic quantum thermometry with germanium-vacancy centers in diamond // ACS Photonics. 2019. V. 6. № 7. P. 1690–1693. https://doi.org/10.1021/acsphotonics.9b00206

10. Cai S., Pan H., González-Vila Á., et al. Selective detection of cadmium ions using plasmonic optical fiber gratings functionalized with bacteria // Opt. Exp. 2020. V. 28. № 13. P. 19740–19749. https://doi.org/10.1364/OE.397505
11. Kavitha B.S., Sridevi S., Makam P., et al. Highly sensitive and rapid detection of mercury in water using functionalized etched fiber Bragg grating sensors // Sensors and Actuators B: Chem. 2021. V. 333. P. 129550. https://doi.org/10.1016/j.snb.2021.129550
12. Li G., Liu Z., Feng J., et al. Pb^{2+} fiber optic sensor based on smart hydrogel coated Mach–Zehnder interferometer // Opt. & Laser Technol. 2022. V. 145. P. 107453. https://doi.org/10.1016/j.optlastec.2021.107453
13. He J., Bell B.A., Casas-Bedoya A., et al. Ultracompact quantum splitter of degenerate photon pairs // Optica. 2015. V. 2. № 9. P. 779–782. https://doi.org/10.1364/OPTICA.2.000779
14. Zhang D., Zhang Z., Wei H., et al. Direct laser writing spiral Sagnac waveguide for ultrahigh magnetic field sensing // Photon. Res. 2021. V. 9. № 10. P. 1984–1991. https://doi.org/10.1364/PRJ.433854
15. Zhang Z., He J., Du B., et al. Miniature optical correlator in a single-nanowire Sagnac loop // ACS Photonics. 2020. V. 7. № 11. P. 3264–3269. https://doi.org/10.1021/acsphotonics.0c01417

AUTHORS

JunQi Guo — Doctor of Engineering, Associate Professor, Chongqing University of Post and Telecommunications, 400065, Chongqing, China; Scopus ID: 55566863500; https://orcid.org/0000-0001-9570-530X; guojq@cqupt.edu.cn

YanFang Zhou — Student, Chongqing University of Post and Telecommunications, 400065, Chongqing, China; Scopus ID: 57660563900; https://orcid.org/0009-0002-3634-1280; 1985430650@qq.com

Yu Liu — Doctor of Engineering, Professor, Chongqing University of Post and Telecommunications, 400065, Chongqing, China; Scopus ID: 55566863500; https://orcid.org/0000-0001-9570-530X; liuyu@cqupt.edu.cn

ChangLe Wang. — Student, Chongqing University of Post and Telecommunications, 400065, Chongqing, China; Scopus ID: 57223168778; https://orcid.org/0009-0000-0137-7473; 1016007806@qq.com

WenYue Zheng. — Student, Chongqing University of Post and Telecommunications, 400065, Chongqing, China; https://orcid.org/0009-0007-2616-2461; 308649700@qq.com

JinLu Jiang. — Student, Chongqing University of Post and Telecommunications, 400065, Chongqing, China; https://orcid.org/0009-0005-8559-0533; 1845426516@qq.com

HanYing Ji. — Student, Chongqing University of Post and Telecommunications, 400065, Chongqing, China; https://orcid.org/0009-0004-4511-3444; 1529978166@qq.com

XiaoYu Chen. — Student, Chongqing University of Post and Telecommunications, 400065, Chongqing, China; https://orcid.org/0009-0004-2846-2028; 1241655631@qq.com

RenPu Li — Doctor of Engineering, Associate Professor, Chongqing University of Post and Telecommunications, 400065, Chongqing, China; Scopus ID: 56316057400; https://orcid.org/0000-0002-0426-296X; lirp@cqupt.edu.cn

The article was submitted to the editorial office 22.02.2023
Approved after review 12.03.2023
Accepted for publication 24.07.2023

Статья поступила в редакцию 22.02.2023
Одобрена после рецензирования 12.03.2023
Принята к печати 24.07.2023